Effects of *Cryptosporidium* infections on host cell metabolome and host mitochondrial associations

Running Title: ***Cryptosporidium*-host metabolomic interactions**

Christopher N. Miller[1], Charalampos G. Panagos[2,6], William R. T. Mosedale[1], Martin Kváč[3,4], Mark J. Howard[2,5] & Anastasios D. Tsaousis[1*]

[1]Laboratory of Molecular & Evolutionary Parasitology, RAPID group, School of Biosciences, University of Kent, Canterbury, UK

[2]Biomolecular NMR facility, School of Biosciences, University of Kent, Canterbury, UK

[3]Institute of Parasitology, Biology Centre CAS, České Budějovice, Czech Republic

[4]Faculty of Agriculture, University of South Bohemia in České Budějovice, České Budějovice, Czech Republic

[5]Centre for Microscopy, Characterisation and Analysis & School of Molecular Sciences, The University of Western Australia, Bayliss Building M313, Perth WA 6009, Australia.

[6]Current address: Complex Carbohydrate Research Center, University of Georgia, Athens, GA, 30602, USA

*** Correspondence:**

Dr. Anastasios D. Tsaousis

A.Tsaousis@kent.ac.uk

Abstract

Cryptosporidium is an important gut microbe whose contributions towards infant and immunocompromise patient mortality rates are steadily increasing. However, current techniques for studying the parasite are few and far between, relying on a combination of *in-silico* predictions and medical reports. The development of an *in-vitro* culture system, using COLO-680N cells (derived from an esophogeal squamous cell carcinoma), has provided the *Cryptosporidium* community with the opportunity to expand its toolkit for investigating this disease. One area in particular that is sorely overlooked is the effect infection has on host metabolic processes, especially those of the host mitochondria, which have been shown anecdotally in previous studies as being in abundance surrounding the sites of infection. Using a ^{1}H Nuclear Magnetic Resonance approach to metabolomics, we have explored the nature of the mouse gut metabolome as well as providing the first insight into the metabolome of an infected cell line. Through a combination of Partial Least Squares Discriminant Analysis and predictive modelling, we demonstrate new understandings of the effects of a *Cryptosporidium* infection, while verifying the presence of known metabolic changes. Of particular note is the potential contribution of host derived taurine to the diuretic aspects of the disease previously attributed to a solely parasite based alteration of the gut environment. This practical and informative approach can spearhead our understanding of the *Cryptosporidium*-host metabolic exchange and thus provide novel targets for tackling this deadly parasite.

Importance

Cryptosporidiosis is a diarrheal disease caused by *Cryptosporidium*, a pathogen of great medical importance. Reports on the infection patterns of the parasite and its interactions with the host are very limited. Using a combination of NMR metabolomics and cell biological techniques, we have shown molecular host-parasite interactions, using both infected mice and the COLO-680N cell line that successfully propagates the parasite. Of major importance are our observations that the host mitochondria have changed their localisation, assembly and production, upon infection by the parasite. Our results also demonstrate further evidence that COLO-680N can be used as a model to investigate these interactions and host manipulation by the parasite. In summary, we present the molecular interactions between *Cryptosporidium* and its host, generate essential knowledge about this medically important pathogen, confirm further the validity of the COLO-680N model of infection and we are providing suggestions of potential new targets for anti-parasitic drug development.

Introduction

Cryptosporidiosis is a disease characterised by prolonged episodes of intense diarrhoea and is the second largest cause of diarrhoeal disease and death in infants across Africa and South Asia, the aetiological agents are apicomplexan parasites: the *Cryptosporidia* (1-4). Cryptosporidiosis is also amongst one of the common diseases of the immunocompromised, particularly HIV positive patients who are at 75-100% risk of contracting the disease during their lifetime, with the specific species of *Cryptosporidium* responsible being either *Cryptosporidium parvum* or *Cryptosporidium hominis* (3, 5-9). Infection occurs when an individual ingests the oocysts of the parasite, often swallowing a contaminated water source. Water treatment options are limited to filtering or boiling, which are generally not possible at an industrial scale and UV treatment, which is both expensive and rarely in place prior to outbreaks. Failing this, treatment is typically rehydration, although one drug has been shown to be effective, the broad spectrum anti-parasitic Nitazoxanide (10). However, the drug is far from ideal and displays a range of undesirable side effects including cytotoxicity and nausea, as well as being limited to use in cases where the patients are immunocompetent (11-14).

Until recently, a significant barrier to research into cryptosporidiosis has been the absence of a combined long-term *in vivo* culturing system and comprehensive model of host parasite interactions in addition to a heavy reliance on antibody based detection both in the scientific and the medical field (2, 4, 12, 15-19). Recent papers have attempted to rectify this by proposing improved or entirely novel techniques for culturing the parasite *ex-vivo* in tissue cultures, using the cultured cancer cells as host cells (18, 20). A recent study identified that infections of COLO-680N cell cultures produced a

longer term and higher production volume culture of the parasite compared to previously existing *in-vitro* cultures (21). These advances have allowed higher in depth microscopy-based studies and even promise to provide a solution to developing a genetic engineering platform for the parasite. However, beyond microscopy and localisation studies, the knowledgebase of the host parasite interaction remains largely undeveloped (4, 13, 14, 22, 23).

One area lacking study is metabolomics. Only two peer-reviewed publications have explored the concept of the infection metabolome, one on mice and the other on human faecal samples, both showing a clear relation between infection and change in metabolite levels (24, 25). While working on different sample sources, each identified the hexadecanoic acid as a significant contributor to the change in the metabolome during infection. Previous studies noticed a number of metabolites, mainly amino acids, decreased in relative abundance in infected mice faeces compared to an increase seen previously in humans (24). This was explained to be most likely due to the inherent variation between the different host species metabolomes, as highlighted by Saric et al. in 2008 and highlights a pressing need for further and wider reaching studies into the metabolome of *Cryptosporidium* infections as well as the development and application of different techniques beyond the Gas Chromatography Mass Spectrometry (GC-MS) used in those papers (24-26).

Currently, the majority of metabolomics studies utilise a GC-MS approach, with great success, however ^{1}H Nuclear Magnetic Resonance (NMR) metabolomics can be used as an additional or alternative powerful tool for metabolic screening. ^{1}H NMR is a simple method that allows for a comparatively lossless analysis of metabolites, with fewer

steps between sample recovery and analysis than GC-MS, which offers a huge advantage for studies involving field samples (26-30). This translates to a more reliable result in terms of quantification and reproducibility. As such, NMR has already seen use in analysing the profile of *Plasmodium falciparum*, although the metabolome of the apicomplexan parasite as a whole is almost entirely unexplored (31).

Here we attempted to investigate the host-parasite interactions, using a combination of microscopy and ^{1}H NMR approaches. In COLO-680N cell biological studies, we observed peculiar interactions between the intracellular, but extracytoplasmic, parasite and its host's mitochondria (21). These observations were even further explored by analysing cryptosporidiosis-induced changes, which we biochemically investigated using a ^{1}H NMR approach. In addition, we have applied the same NMR based methodology to infected mice guts, in order to study the similarities and differences displayed between *in-vivo* and *in-vitro* models and identify potential cross-species markers of infection.

Results

Host mitochondria during infection

To investigate the cellular role of host organelles during infection, we employed an Indirect Fluorescence Assay (IFA) approach to determine whether the organelles, particularly the mitochondria, of the host cells were responding to a *Cryptosporidium* infection **(Figure 1)**. Our results demonstrated that on multiple occasions, approximating 80-90% of infected cells, the host mitochondria were shown to

congregate in larger densities near the *Cryptosporidium* infection, with a corresponding increase in labelling intensity compared to uninfected areas, indicative of stronger mitochondrial metabolic activity (**Figures 1; Videos 1-3**). Transmission Electron Microscopy images of infected cells also showed host mitochondrial congregation around the parasitophorous vacuole (**Figure 2**). Interestingly, in infected cell cultures we observed, cytoskeletal structures (either actin or tubulin) were seen to conjugate with the host mitochondria, “pulling” them around the parasitophorous vacuole, in response to the infection by the parasite.

Cell culture sample extractions

Extrapolated NMR data from COLO-680N (n = 38, *C. parvum* Iowa = 12, Control = 12, *C. hominis* = 7, *C. parvum* Weru = 7) metabolite extractions, demonstrated clear differences between the *Cryptosporidium* used in comparison to both the control and other infections; each set of spectra within a group appeared visually identical both between each individual sample and their technical repeats, indicating reliable spectra acquisition (**Figure 3a**). Readily visible differences could be seen between creatine, creatine phosphate, taurine and lactate (**Figures 3b-d**) were readily visible in the raw spectra. Chenomx analysis produced a list of 161 total compounds of varying concentrations across samples (**Figure 4**). The PCA generated by the same statistical analysis as before, produced ample separation of the *Cryptosporidium*-infected and uninfected cultures in multiple experiments (**Figure 5a and 5c)**. Furthermore, the separation of the individual infection groups suggests that differences between both *Cryptosporidium* species and within individual strains of *C. parvum,* may illicit different

metabolic responses in cell cultures. It is important to note that all data obtained from the 38 individual samples was input into the calculations, as there was insufficient evidence to suggest any were statistical outliers. The loading scores plot of the PCA showed a number of amino acids contributed heavily to the separations between groups, such as lactate, several fatty acid derivatives and taurine (**Figure 5b**).

Any and all metabolites identified in this manner were input into an online tool (MetaboAnalyst 3.0) producing a graph detailing which metabolic pathways were influenced by infection (**Figure 6a**) (32). This approach identified several pathways, including the biosynthesis of various amino acids, as well as ketones and CoA (**Figure 6b-f**). Within these pathways, metabolites were highlighted that were identified via the PCA as contributing reliably towards differences between groups. Full compound names are available in **Supplementary Figure 1**.

Mice faecal sample extractions

Faecal samples from infected and uninfected mice were smeared onto microscope slides and stained with a aniline-carbol-methyl violet method, allowing the detection of *C. parvum* oocysts and thus validation of successful infections (**Supplementary Figure 2**). Samples from both control and infected mice were taken at ten days' post infection. The spectra produced by the NMR showed clear distinctions between the infected and uninfected mice, as well as distinctions between the different strains of infections (**Figure 7a**). Though 38 individual experiments were used to produce this data, the validity and reliability of each was confirmed by performing a further 9 technical replicate NMR scans. Several metabolites were readily distinguishable prior to the metabolomics analyses, including indicators of phosphorylation; taurine (**Figure 7b**), creatine and

creatine phosphate (**Figure 7c**) and lactate (**Figure 7d**). Processing the data from the mice guts (n = 18, six per infection) via the Chenomx Nmr Suite version 8.2 platform produced a list of 151 compounds that were extrapolated from the spectra (**Figure 8**). Statistical analysis of the data, with freely available Microsoft Excel Add-in "multi-base 2015", by Partial Least Squares Discriminant Analysis (PLS-DA) determined notable separation of the three conditions, (uninfected control, *C. parvum* Iowa II and *C. parvum* Weru infections), whilst maintaining group cohesion (**Figure 9a**). The loading values of the variable compound contributions (**Figure 9b**), suggest certain metabolites were more significant to the separation of the groups than others. The presence of L-alanine and valine, two common amino acids, agrees with the previous literature and 2-oxoisocaproate is a component of the valine/leucine/isoleucine biosynthetic pathways reports (24, 25).

MetaboAnalyst 3.0 based analysis of the metabolites proposed that a number of amino acid biosynthesis pathways could be altered during the course of an infection, such as the glycine, valine and taurine pathways. In addition, the mice infections displayed possible changes to other metabolic pathways (**Figure 10a)** as those pathways furthest from the x, y axis intercept, representing both the overall completeness of the pathways and number of contributing detected metabolites respectively. As with **Figures 6a-g,** the pathways identified in the manner, and the compounds discovered by the NMR demonstrated that infections caused changes in at least the valine (**Figure 10c**), glycine (**Figure 10d**) and taurine amino (**Figure 10e**) acid biosynthetic pathways, in addition to several sugar pathways (**Figure 10b, f, g**). As before, full compound names are available in **Supplementary Figure 1**.

Comparison of mice faecal and COLO-680N metabolome changes

MetaboAnalyst data from **Figure 6** and **Figure 10,** demonstrate that a number of altered pathways are shared between the mice and tissue culture metabolites, particularly taurine and amino acid metabolic pathways. Taurine is involved in a number of roles, including bile acid conjugation, osmoregulation, membrane integrity and protection against oxidative free radicals. Glycine synthesis was also shown to be affected to a large degree and is involved with numerous and diverse cellular functions including purine synthesis, basic protein construction and provides the building blocks for porphyrins (33, 34). All of these pathways have a direct or indirect impact on the host's mitochondrial energetic activity. Comparing the data from the mouse and cell culture responses directly revealed a large number of metabolite level responded similarly to infection regardless of host (**Figures 11a and b)**. Interestingly, although the mitochondria remained the most likely site of metabolic change, regardless of host or parasite, the metabolites in question did change depending on the parasite strain involved.

Discussion

Previous studies (21) recently demonstrated the successful long-term propagation of *Cryptosporidium parvum* in COLO-680N cell culture. Their studies have shown the presence of organelles around the parasite (e.g. feeder organelle), which implied a direct association between the parasite and the host. This host-parasite relation became

more intriguing when we observed a close relation between the host mitochondria and the parasite during infection. To investigate this even further, we have used a combination on mitochondrial assays, which have shown higher mitochondrial activity in infected cells and ^{1}H NMR to explore the metabolomics of the infection.

Solution-state ^{1}H NMR offers a practical approach to metabolomics that is especially useful where sample volume sizes are particularly small (27, 30, 35). Although GC-MS holds an advantage for detecting low-levels of metabolites with unique mass signatures, for the purpose of determining the change in metabolite quantities, NMR provides a viable alternative (26-31). Initial analysis of our data showed a clear distinction between the metabolic fingerprints of infected and uninfected samples, even between infections of different strains of the parasite to some extent; with PCA producing distinct groups of metabolite profiles, correlating to uninfected and infected samples (**Figure 5a and c**). This may in-part be explained as the manifestation of the biochemical differences between the species which contribute to their observed species specificity

Of particular importance is the degree to which these results, both from the *in-vitro* and *in-vivo*, agree with the previous literature. Our study also demonstrates that metabolic compounds L-alanine, isoleucine and succinic acid (succinate) were detected as contributors to the variance between the sample conditions that indicated infection. Moreover, even though valine was not detected in the uninfected controls, it was visible in the infected samples and in agreement with previous studies (24, 25).

The MetaboAnalyst data revealed a number of pathways were potentially influenced by infection, including several that showed changes in both the mice and cell culture experiments, such as amino acid and CoA biosynthesis. Support for these findings is

observed via the biosynthesis pathways for alanine and glycine that were highlighted previously in GC-MS studies as being potentially influenced by infection (24, 25)

As a parasite, *Cryptosporidium* is dependent on host derived biosynthetic pathways for survival. For example, *C. parvum* is incapable of producing the majority of amino acids *de-novo*, instead relying heavily on the import of host metabolites via active channelling (36). The biosynthetic pathway for glycine, threonine and serine was upregulated, in both cell culture and animal experimentations, with particularly high levels of glycine detected. Both *C. parvum* and *C. hominis* are incapable of manufacturing these amino acids *de novo*, instead relying on scavenging host serine and glycine, utilising serine and glycine hydroxymethyltransferases to convert one to the other when needed (36, 37). The reliance on host amino acids could provide a novel method for combating the infection, based upon previous studies that identified other amino acid metabolic chains as potential targets (37, 38). For example, glycine reuptake inhibitors (GRIs) that are often used in treating schizophrenia, could be utilised to partially starve the parasite of the metabolite.

In addition to the amino acid biosynthesis pathways, it is also apparent that taurine synthesis is also implicated in the metabolic profile of the disease as shown in the presented analyses; taurine has frequently been used in the past as an agent for inducing excystation for *in-vitro* cultures as sodium taurochloate (39-42). In the host, taurine has a number of roles, those relevant to the cell types involved include: cell membrane integrity, osmoregulation and adipose tissue regulation. Previous metabolomic studies of faecal samples from *Cryptosporidium*-infected patients revealed increased taurine concentrations, explained by the characteristic decline in gut

absorption as a result of villi malformation by the parasite (43, 44). However, an even greater increase in taurine levels was observed in the infected COLO-680N cell cultures, wherein malabsorption is not an applicable explanation. In addition to the pathways and the relevant metabolites featured in **Figures 6** and **10,** there were also a number of potentially important metabolites not represented. Increases were also observed in the abundance of adenosine derivatives (AMP, ADP and ATP); all showing an increased abundance in infected cells and mice in *C. parvum* Iowa II infections, along with a similar increase in creatine levels in *C. parvum* Weru infections. This implicates the role of host mitochondria in the context of infection as each species and strain used lacks the creatine kinase needed to produce creatine phosphate, which typically operate in localisation with mitochondria. Levels of pyruvate in *C. hominis* cell and pantothenate in *C. parvum* Iowa II infections suggest a role for oxidatative phosphorylation. This is of particular interest as the *C. parvum* genome contains a sequence for a potential pantothenate scavenging protein (45). Moreover, the further increase in lactate levels detected in *C. hominis* cell cultures and *C. parvum* Iowa II mouse infected samples, compared to the controls, indicate a strong contribution from anaerobic pathways most likely from the host. This suggests that more ATP is being produced than the oxidative capacity of the host mitochondria can maintain, producing a net increase in lactate as the oxygen debt increases. Similar observations have been made in other intracellular parasites, including the microsporidian *Encephalitozoon cuniculi*, in which the organism acquired specialized transporters to overcome its needs for ATP (46).

These data suggest that *C. parvum* and *C. hominis* infections may be directly or indirectly inducing an increase in host mitochondrial activity. If factual, this would result in a large number of oxygen free radicals being produced by the metabolic machinery. Consequently, cell(s) would respond with a matching increase in the synthesis of antioxidants such as taurine, which also sees increases during infection (47-49). Support for this hypothesis can be seen in the way host mitochondria appear to congregate around the *Cryptosporidium* infection (e.g. parasitophorous vacuole) (**Figures 1** and **2)**. Nevertheless, taurine also plays another role within cells, for example as a diuretic. Taurine is involved in the maintenance of the ionised forms of magnesium and potassium within the cell, producing a diuretic effect that may contribute towards the characteristic water-loss of a patient with cryptosporidiosis (43, 50-52). Furthermore, it has been found that taurine levels influence production of short chained fatty acid, another aspect of host biology theorised to be scavenged by *C. parvum* and *C. hominis* (52-54). The detection of a rise in taurine levels *in-vitro* further suggest that the increase in taurine typically detected in cryptosporidiosis patients' stool, is more than simply the result of the guts decrease in absorptive qualities. It is likely that the intra-cellular role of taurine in this disease has been overlooked and that the pathophysiology of this disease is more complicated than currently understood, and extends beyond simple villi degradation.

Lastly, these results alone suggest the option of determining infections via a possible comparative ^{1}H NMR of patient and reference biopsies. This method offers an alternative approach in the medical field, where current methods of diagnosis are reliant on separate methods to achieve the same result as NMR, with infections detected by

318 laborious and often inaccurate microscopy and strain typing dependant on successful
319 PCR.

320 In conclusion, we have demonstrated for the first time that the use of ^{1}H NMR in the
321 context of both medical and scientific applications is indispensable in the fight against
322 cryptosporidiosis. With the application of a more user-friendly and reproducible
323 approach of metabolomics, through the ^{1}H NMR methodology described in this paper, it
324 will now be easier for the *Cryptosporidium* community to further explore the remaining
325 aspects of the disease metabolome in patients' samples. Future experiments could
326 include similar investigations of other *Cryptosporidium* species and their published *in*
327 *vitro* cell cultures or an in-depth analysis of one of the many compounds identified in this
328 paper. Additionally, elucidating the more pathogenic influences of taurine biosynthesis
329 in the pathobiology of cryptosporidiosis is critical. With these data, a metabolomics
330 based method of diagnosing and treating the disease could become a reality.

331

332 **Materials and Methods**

333 *Cryptosporidium*

334 Three isolates of *C. parvum* were used in this study. The reference strain *C. parvum*
335 Iowa II was obtained from Bunch Grass Farm in the United States, isolated from
336 infected calves. The human isolate *C. parvum* Weru strain was supplied courtesy of Dr
337 Martin Kváč of the Institute of Parasitology Biology Centre CAS, Czech Republic. The
338 Weru strain was originally isolated from an infected human patient and subsequently
339 maintained by passing through SCID mice. The final isolate used was the human isolate

of *C. hominis*, supplied courtesy of Prof. Rachel Chalmers from the *Cryptosporidium* Reference Unit, Singleton Hospital of NHS Wales.

Tissue culture

75 cm^2 monolayers of COLO-680N were infected and maintained as per the protocols outlined previously (21), using all three isolates of *Cryptosporidium*. A control group was also established, following the same protocols as the infections, absent oocysts. Two separate experiments were executed using a minimum of five flasks per sample condition.

Animals and infection

For this study, seven day old BALB/c mice were infected at the Institute of Parasitology, Biology Centre CAS using pre-established protocols detailed in Meloni and Thompson, totalling five mice per condition (55). Balb/c were chosen due to their similar response to infection as a healthy adult male. Three separate conditions, totaling six animal each, were used, infecting with 100,000 oocysts of *C. parvum* Iowa II, 100,000 oocysts of the *C. parvum* Weru isolate or a PBS control, given by oral gavage. The groups were kept physically separated and never allowed to interact. Infection was monitored from Day-1 post-infection by aniline-carbol-methyl violet staining of faecal smears staining of faecal smears, in addition to an antigen based strip test (56), RIDA®QUICK *Cryptosporidium*, supplied by R-Biopharm. At ten days' post-infection, the mice were euthanized by cervical dislocation and decapitation. Samples of the ileum were dissected from the mice, measured to the same size to ensure reproducibility. This study was carried out in accordance with Act No 246/1992 Coll. of the Czech Republic. The protocol was

approved by the Committee for Animal Welfare of Biology Centre Czech Academy of Science and the veterinary administration authorities with regards to the animal experiments, (experiment reference numbers: 114/2013 and 52/2014).

Sample preparation for NMR

The following protocol was adapted from published and well-established metabolic extraction methods used for NMR-based untargeted analysis of cell extracts (57-60). Animal samples were retrieved from the contents of the ileum and surrounding intestinal structure by dissecting out the area of interest and washing through with 3 ml 100% ethanol at room temperature via syringe inserted into the opening, collecting the wash through.

Collected samples were then centrifuged for three minutes at 10,000 *g*, the supernatant discarded and the pellet weights recorded. The samples were then suspended by vortex in 2 ml of 75% ethanol, pre-heated to 80°C, to immediately inhibit subsequent metabolic reactions, then transferred to a new tube and an additional five ml of 75% ethanol added.

2 ml of 2 mm diameter glass beads were added to the samples and agitated by vortex for 30 seconds before incubating the samples for three minutes at 80°C. The samples were vortexed for a further 30 seconds or until the sample was completely homogenised. Tissue culture samples were collected by draining the media, adding 6 ml of ethanol at 80°C to the culture flask and scraping the cells off the surface by cell scraper, transferring the mixture of lysed cells into 15 ml polyethylene tubes via a 10-ml serological pipette.

384 The samples were then transferred into 2 ml tubes, retaining the glass beads in 15 ml
385 conical tubes. The beads were washed with an additional two ml of 80°C, 75% ethanol
386 and again the liquid was transferred into sterile 2 ml tubes, retaining the glass beads in
387 the tube.

388 Cell debris and general detritus were removed from the samples by centrifugation at
389 16,000 *g* for 10 minutes and the resulting supernatant transferred to new, sterile 2 ml
390 microcentrifuge tubes. The samples were then dried via Rotorvac for 12 hours or until
391 completely desiccated, at 40°C, suspended in 330 µl double distilled water and
392 centrifuged at 2,500 *g* for 10 minutes. The supernatants were recombined into ~1 ml
393 aliquots per original sample in sterile 1.5 ml microcentrifuge tubes and frozen at -20 °C
394 until the day before NMR analysis. The sample tubes are subsequently placed into a
395 freeze drier until completely desiccated, suspended in 1 ml of deuterium oxide (^2H_2O)
396 and spiked with the sodium salt of the calibration and quantitation control compound: 3-
397 (Trimethylsilyl)-1-propanesulfonic acid (DSS), to a final concentration of 20 µM and a
398 tested pH of 7.5.

399 *NMR protocol and analysis*

400 Samples were analysed using a 4-channel Bruker Avance III 14.1 T NMR spectrometer
401 (600 MHz ^1H) equipped with a 5 mm QCI-F cryoprobe. For controls: six separate,
402 uninfected 25 cm^2 COLO-680N 100% confluent monolayer cultures were analysed in
403 addition to three uninfected BALB/c mice. Infected samples consisted of six 25 cm^2
404 COLO-680N 100% confluent monolayers in addition to three Iowa infected BALB/c and
405 three Weru infected BALB/c mice. One dimension NMR datasets were acquired with a
406 pulse repetition rate of 5 s over 128 scans, preceded by eight equilibrating dummy

scans and suppression of the residual Deuterium Oxide solvent (HDO) resonance using presaturation. This was repeated 5 times per sample in order to ensure the reliability of the spectra produced. Processed NMR spectrographic datasets were produced by Topspin 3.2 and analysed using Chenomx NMR Suite version 8.2. Partial Least Squares Discriminant Analysis (PCA) of the Chenomx data were generated with the freely available Microsoft Excel Add-in “multi-base 2015” by Numerical Dynamics, Japan (61) and “Past3.x” by Øyvind Hammer, Natural History Museum, University of Oslo. Pathway predictions were produced by the MetaboAnalyst 3.0 web tool, using a hypergeometric test and relative-betweeness centrality against *Homo sapiens* and *Mus musculus* databases for the tissue culture and mouse models respectively (32).

Indirect Fluorescence Assays

COLO-680N cultures were seeded onto Lab-Tek, two well, Permanox chamber slides (Sigma Aldrich, Cat No. Z734640) and allowed to reach 70% confluence before infecting, following previously published protocols (21). At seven days post infection the media was aspirated from the cultures and washed twice with 1 x PBS. Fresh, pre-warmed RPMI-1640 (Sigma Aldrich, Cat. No R8758) (1% Antibiotic/Antimycotic) containing 200 nM Thermofisher Mitotracker Red CMXRos (Molecular probes; Cat. No M7512), was added to the wells and incubated in the dark at 37°C for 45 minutes. The media was removed and replaced with further pre-warmed RPMI-1640 (1% Antibiotic/Antimycotic), containing 3.5% formaldehyde, for 15 minutes at 37°C as per the manufacturer’s protocol. The cells were then briefly permeabilised with 0.2% Triton-x100 in 1x PBS for 10 minutes, washed twice with 1x PBS and four drops of SporoGlo™ (sensitive to *Cryptosporidium* life cycle stages, excluding the oocyst) or

Crypt-a-glo™ (WATERBORNE, INC) (less sensitive to intracellular life cycle stages but sensitive for oocyst proteins) added, with incubation at 37°C for a further 45 minutes. The final sample was then washed three times with PBS, dried and Fluoroshield™ with DAPI (Sigma Aldrich, Cat. No F6057) was added before applying a glass coverslip and sealing. Slides were visualised by fluorescence microscopy using an Olympus IX82 or Zeiss Elyra P1 confocal microscope.

Electron microscopy images

Aclar disks of tissue culture were infected and prepared for EM according to the protocols detailed previously (21).

Ethics Statement

This study was carried out in accordance with Act No 246/1992 Coll. of the Czech Republic. 419 The protocol was approved by the Committee for Animal Welfare of Biology Centre Czech 420 Academy of Science and the veterinary administration authorities with regards to the animal 421 experiments (experiment reference numbers: 114/2013 and 52/2014).

Abbreviations

NMR: Nuclear Magnetic Resonance

DSS: 3-(Trimethylsilyl)-1-propanesulfonic acid, sodium salt

PCA: Principal component analysis

PLS-DA: Partial Least Squares Discriminant Analysis

UV: Ultraviolet

HIV: Human Immunodeficiency Virus

GC-MS: Gas Chromatography-Mass Spectrometry

HDO: Deuterium Oxide

IFA: Indirect Fluorescence Assay

PCR: Polymerase Chain Reaction

DAPI: 4',6-diamidino-2-phenylindole

PBS: Phosphate-buffered saline

EM: Electron microscopy

SCID: Severe Combined Immunodeficiency Disease

ATP: adenosine triphosphate

AMP: adenosine monophosphate

ADP: adenosine diphosphate

CoA: Coenzyme A

GRIs: glycine reuptake inhibitors

Declarations

The authors have declared that the research was conducted in the absence of any commercial or financial relationships that could be construed as a potential conflict of interest

Funding was provided by the BBSRC, Wellcome Trust and a Microbiology Society Research Visit Grant.

Acknowledgements

This research was supported by BBSRC research grant (BB/M009971/1) to Dr. Anastasios Tsaousis and a Wellcome Trust Equipment Grant 091163/Z/10/Z to Dr. Mark J. Howard. Christopher N. Miller is supported by a GTA studentship from the School of Biosciences, University of Kent and a Research Visit Grant award from the Microbiology Society. Martin Kvac is supported by The Czech Science Foundation (project No. 15-01090S). We thank Dr. Michelle Rowe for NMR technical support at Kent and members of the Dr. Tsaousis and Dr. Kvac laboratories for their intellectual and methodological support. We would also like to thank Matthew Lee and Matthew D. Badham from the University of Kent for the assistance in using the confocal microscope and analysing data.

References:

1. Kotloff KL, Nataro JP, Blackwelder WC, Nasrin D, Farag TH, Panchalingam S, Wu Y, Sow SO, Sur D, Breiman RF, Faruque AS, Zaidi AK, Saha D, Alonso PL, Tamboura B, Sanogo D, Onwuchekwa U, Manna B, Ramamurthy T, Kanungo S, Ochieng JB, Omore R, Oundo JO, Hossain A, Das SK, Ahmed S, Qureshi S, Quadri F, Adegbola RA, Antonio M, Hossain MJ, Akinsola A, Mandomando I, Nhampossa T, Acacio S, Biswas K, O'Reilly CE, Mintz ED, Berkeley LY, Muhsen K, Sommerfelt H, Robins-Browne RM, Levine MM. 2013. Burden and aetiology of diarrhoeal disease in infants and young children in developing countries (the Global Enteric Multicenter Study, GEMS): a prospective, case-control study. Lancet 382:209-22.
2. Checkley W, White AC, Jr., Jaganath D, Arrowood MJ, Chalmers RM, Chen XM, Fayer R, Griffiths JK, Guerrant RL, Hedstrom L, Huston CD, Kotloff KL, Kang G, Mead JR, Miller M, Petri WA, Jr., Priest JW, Roos DS, Striepen B, Thompson RC, Ward HD, Van Voorhis WA, Xiao L, Zhu G, Houpt ER. 2014. A review of the global burden, novel diagnostics, therapeutics, and vaccine targets for cryptosporidium. Lancet Infect Dis 15:85-94.
3. Wanyiri JW, Kanyi H, Maina S, Wang DE, Steen A, Ngugi P, Kamau T, Waithera T, O'Connor R, Gachuhi K, Wamae CN, Mwamburi M, Ward HD. 2014. Cryptosporidiosis in HIV/AIDS patients in Kenya: clinical features, epidemiology, molecular characterization and antibody responses. Am J Trop Med Hyg 91:319-28.

4. Striepen B. 2013. Parasitic infections: Time to tackle cryptosporidiosis. Nature 503:189-91.
5. Shirley DA, Moonah SN, Kotloff KL. 2012. Burden of disease from cryptosporidiosis. Curr Opin Infect Dis 25:555-63.
6. Caccio SM. 2005. Molecular epidemiology of human cryptosporidiosis. Parassitologia 47:185-92.
7. Leoni F, Amar C, Nichols G, Pedraza-Diaz S, McLauchlin J. 2006. Genetic analysis of *Cryptosporidium* from 2414 humans with diarrhoea in England between 1985 and 2000. J Med Microbiol 55:703-7.
8. Wielinga PR, de Vries A, van der Goot TH, Mank T, Mars MH, Kortbeek LM, van der Giessen JWB. 2008. Molecular epidemiology of *Cryptosporidium* in humans and cattle in The Netherlands. International Journal for Parasitology 38:809-817.
9. Widmer G, Sullivan S. 2012. Genomics and population biology of *Cryptosporidium* species. Parasite Immunol 34:61-71.
10. Doumbo O, Rossignol JF, Pichard E, Traore HA, Dembele TM, Diakite M, Traore F, Diallo DA. 1997. Nitazoxanide in the treatment of cryptosporidial diarrhea and other intestinal parasitic infections associated with acquired immunodeficiency syndrome in tropical Africa. Am J Trop Med Hyg 56:637-9.
11. Hussien SM, Abdella OH, Abu-Hashim AH, Aboshiesha GA, Taha MA, El-Shemy AS, El-Bader MM. 2013. Comparative study between the effect of nitazoxanide and paromomycine in treatment of cryptosporidiosis in hospitalized children. J Egypt Soc Parasitol 43:463-70.

534 12. Domjahn BT, Hlavsa MC, Anderson B, Schulkin J, Leon J, Jones JL. 2014. A
535 survey of U.S. obstetrician-gynecologists' clinical and epidemiological knowledge
536 of cryptosporidiosis in pregnancy. Zoonoses Public Health 61:356-63.
537 13. Sparks H, Nair G, Castellanos-Gonzalez A, White AC, Jr. 2015. Treatment of
538 Cryptosporidium: What We Know, Gaps, and the Way Forward. Curr Trop Med
539 Rep 2:181-187.
540 14. Manjunatha UH, Chao AT, Leong FJ, Diagana TT. 2016. Cryptosporidiosis Drug
541 Discovery: Opportunities and Challenges. ACS Infect Dis 2:530-7.
542 15. Leitch GJ, He Q. 2012. Cryptosporidiosis-an overview. J Biomed Res 25:1-16.
543 16. Briggs AD, Boxall NS, Van Santen D, Chalmers RM, McCarthy ND. 2014.
544 Approaches to the detection of very small, common, and easily missed outbreaks
545 that together contribute substantially to human *Cryptosporidium* infection.
546 Epidemiol Infect 142:1869-76.
547 17. Karanis P, Aldeyarbi HM. 2011. Evolution of *Cryptosporidium* in vitro culture. Int J
548 Parasitol 41:1231-42.
549 18. Muller J, Hemphill A. 2013. In vitro culture systems for the study of apicomplexan
550 parasites in farm animals. Int J Parasitol 43:115-24.
551 19. Girouard D, Gallant J, Akiyoshi DE, Nunnari J, Tzipori S. 2006. Failure to
552 propagate Cryptosporidium spp. in cell-free culture. J Parasitol 92:399-400.
553 20. Morada M, Lee S, Gunther-Cummins L, Weiss LM, Widmer G, Tzipori S, Yarlett
554 N. 2016. Continuous culture of *Cryptosporidium parvum* using hollow fiber
555 technology. Int J Parasitol 46:21-9.

21. Miller CN, Jossé L, Brown I, Blakeman B, Povey J, Yiangou L, Price M, Cinatl jr J, Xue W-F, Michaelis M, Tsaousis AD. 2017. A cell culture platform for *Cryptosporidium* that enables long-term cultivation and new tools for the systematic investigation of its biology. Int J Parasitol in press.

22. Sponseller JK, Griffiths JK, Tzipori S. 2014. The evolution of respiratory Cryptosporidiosis: evidence for transmission by inhalation. Clin Microbiol Rev 27:575-86.

23. Wilhelm CL, Yarovinsky F. 2014. Apicomplexan infections in the gut. Parasite Immunol 36:409-20.

24. Ng Hublin JSY, Ryan U, Trengove RD, Maker GL. 2012. Development of an untargeted metabolomics method for the analysis of human faecal samples using *Cryptosporidium*-infected samples. Molecular and Biochemical Parasitology 185:145-150.

25. Ng Hublin JS, Ryan U, Trengove R, Maker G. 2013. Metabolomic profiling of faecal extracts from *Cryptosporidium parvum* infection in experimental mouse models. PLoS One 8:e77803.

26. Saric J, Wang Y, Li J, Coen M, Utzinger J, Marchesi JR, Keiser J, Veselkov K, Lindon JC, Nicholson JK, Holmes E. 2008. Species variation in the fecal metabolome gives insight into differential gastrointestinal function. J Proteome Res 7:352-60.

27. Jacobs DM, Deltimple N, van Velzen E, van Dorsten FA, Bingham M, Vaughan EE, van Duynhoven J. 2008. (1)H NMR metabolite profiling of feces as a tool to assess the impact of nutrition on the human microbiome. NMR Biomed 21:615.

28. Bezabeh T, Somorjai RL, Smith ICP. 2009. MR metabolomics of fecal extracts: applications in the study of bowel diseases. Magnetic Resonance in Chemistry 47:S54-S61.

29. Hong YS, Ahn YT, Park JC, Lee JH, Lee H, Huh CS, Kim DH, Ryu DH, Hwang GS. 2010. 1H NMR-based metabonomic assessment of probiotic effects in a colitis mouse model. Arch Pharmacal Res 33:1091.

30. Wu J, An Y, Yao J, Wang Y, Tang H. 2010. An optimized sample preparation method for NMR-based faecal metabonomic analysis. Analyst 135:1023.

31. Sengupta A, Ghosh S, Das BK, Panda A, Tripathy R, Pied S, Ravindran B, Pathak S, Sharma S, Sonawat HM. 2016. Host metabolic responses to Plasmodium falciparum infections evaluated by 1H NMR metabolomics. Mol Biosyst.

32. Xia J, Sinelnikov IV, Han B, Wishart DS. 2015. MetaboAnalyst 3.0--making metabolomics more meaningful. Nucleic Acids Res 43:W251-7.

33. Denis V, Daignan-Fornier B. 1998. Synthesis of glutamine, glycine and 10-formyl tetrahydrofolate is coregulated with purine biosynthesis in *Saccharomyces cerevisiae*. Molecular and General Genetics MGG 259:246-255.

34. Marver HS, Tschudy DP, Perlroth MG, Collins A. 1966. Delta-aminolevulinic acid synthetase. I. Studies in liver homogenates. J Biol Chem 241:2803-9.

35. Novak P, Tepes P, Fistric I, Bratos I, Gabelica V. 2006. The application of LC-NMR and LC-MS for the separation and rapid structure elucidation of an unknown impurity in 5-aminosalicylic acid. J Pharm Biomed Anal 40:1268.

601 36. Abrahamsen MS, Templeton TJ, Enomoto S, Abrahante JE, Zhu G, Lancto CA,
602 Deng M, Liu C, Widmer G, Tzipori S, Buck GA, Xu P, Bankier AT, Dear PH,
603 Konfortov BA, Spriggs HF, Iyer L, Anantharaman V, Aravind L, Kapur V. 2004.
604 Complete genome sequence of the apicomplexan, *Cryptosporidium parvum*.
605 Science 304:441-5.
606 37. Doyle PS, Kanaani J, Wang CC. 1998. Hypoxanthine, guanine, xanthine
607 phosphoribosyltransferase activity in *Cryptosporidium parvum*. Exp Parasitol
608 89:9-15.
609 38. Clark DP. 1999. New Insights into Human Cryptosporidiosis. Clinical
610 Microbiology Reviews 12:554-563.
611 39. Feng H, Nie W, Sheoran A, Zhang Q, Tzipori S. 2006. Bile acids enhance
612 invasiveness of *Cryptosporidium* spp. into cultured cells. Infect Immun 74:3342-6.
613 40. Gold D, Stein B, Tzipori S. 2001. The utilization of sodium taurocholate in
614 excystation of *Cryptosporidium parvum* and infection of tissue culture. J Parasitol
615 87:997-1000.
616 41. Kar S, Daugschies A, Cakmak A, Yilmazer N, Dittmar K, Bangoura B. 2011.
617 Cryptosporidium parvum oocyst viability and behaviour of the residual body
618 during the excystation process. Parasitol Res 109:1719-23.
619 42. King BJ, Keegan AR, Phillips R, Fanok S, Monis PT. 2012. Dissection of the
620 hierarchy and synergism of the bile derived signal on *Cryptosporidium parvum*
621 excystation and infectivity. Parasitology 139:1533-46.

622 43. Kapembwa MS, Bridges C, Joseph AE, Fleming SC, Batman P, Griffin GE. 1990.
623 Ileal and jejunal absorptive function in patients with AIDS and enterococcidial
624 infection. J Infect 21:43-53.
625 44. Goodgame RW, Kimball K, Ou C-N, White AC, Genta RM, Lifschitz CH, Chappell
626 CL. 1995. Intestinal function and injury in acquired immunodeficiency
627 syndrome—related cryptosporidiosis. Gastroenterology 108:1075-1082.
628 45. Augagneur Y, Jaubert L, Schiavoni M, Pachikara N, Garg A, Usmani-Brown S,
629 Wesolowski D, Zeller S, Ghosal A, Cornillot E, Said HM, Kumar P, Altman S, Ben
630 Mamoun C. 2013. Identification and functional analysis of the primary
631 pantothenate transporter, PfPAT, of the human malaria parasite *Plasmodium*
632 *falciparum*. J Biol Chem 288:20558-67.
633 46. Tsaousis AD, Kunji ERS, Goldberg AV, Lucocq JM, Hirt RP, Embley TM. 2008. A
634 novel route for ATP acquisition by the remnant mitochondria of *Encephalitozoon*
635 *cuniculi*. Nature 453:553-556.
636 47. Giris M, Depboylu B, Dogru-Abbasoglu S, Erbil Y, Olgac V, Alis H, Aykac-Toker
637 G, Uysal M. 2008. Effect of taurine on oxidative stress and apoptosis-related
638 protein expression in trinitrobenzene sulphonic acid-induced colitis. Clin Exp
639 Immunol 152:102.
640 48. Green TR, Fellman JH, Eicher AL, Pratt KL. 1991. Antioxidant role and
641 subcellular location of hypotaurine and taurine in human neutrophils. Biochim
642 Biophys Acta 1073:91-7.

643 49. Zhang M, Izumi I, Kagamimori S, Sokejima S, Yamagami T, Liu Z, Qi B. 2004.
644 Role of taurine supplementation to prevent exercise-induced oxidative stress in
645 healthy young men. Amino Acids 26:203-7.
646 50. Lin S, Sanders DS, Gleeson JT, Osborne C, Messham L, Kurien M. 2016. Long-
647 term outcomes in patients diagnosed with bile-acid diarrhoea. Eur J
648 Gastroenterol Hepatol 28:240-5.
649 51. Niggli V, Sigel E, Carafoli E. 1982. Inhibition of the purified and reconstituted
650 calcium pump of erythrocytes by micro M levels of DIDS and NAP-taurine. FEBS
651 Lett 138:164-6.
652 52. Yu H, Guo Z, Shen S, Shan W. 2016. Effects of taurine on gut microbiota and
653 metabolism in mice. Amino Acids 48:1601-17.
654 53. Seeber F, Soldati-Favre D. 2010. Metabolic pathways in the apicoplast of
655 apicomplexa. Int Rev Cell Mol Biol 281:161-228.
656 54. Guo F, Zhang H, Payne HR, Zhu G. 2016. Differential Gene Expression and
657 Protein Localization of *Cryptosporidium parvum* Fatty Acyl-CoA Synthetase
658 Isoforms. J Eukaryot Microbiol 63:233-46.
659 55. Meloni BP, Thompson RC. 1996. Simplified methods for obtaining purified
660 oocysts from mice and for growing *Cryptosporidium parvum* in vitro. J Parasitol
661 82:757-62.
662 56. Milacek P, Vitovec J. 1985. Differential staining of cryptosporidia by aniline-
663 carbol-methyl violet and tartrazine in smears from feces and scrapings of
664 intestinal mucosa. Folia Parasitol (Praha) 32:50.

57. Tarrant DJ, Stirpe M, Rowe M, Howard MJ, von der Haar T, Gourlay CW. 2016. Inappropriate expression of the translation elongation factor 1A disrupts genome stability and metabolism. Journal of Cell Science 129:4455-4465.

58. Bastow EL, Peswani AR, Tarrant DS, Pentland DR, Chen X, Morgan A, Staniforth GL, Tullet JM, Rowe ML, Howard MJ, Tuite MF, Gourlay CW. 2016. New links between SOD1 and metabolic dysfunction from a yeast model of amyotrophic lateral sclerosis. J Cell Sci 129:4118-4129.

59. Holyoake LV, Hunt S, Sanguinetti G, Cook GM, Howard MJ, Rowe ML, Poole RK, Shepherd M. 2016. CydDC-mediated reductant export in Escherichia coli controls the transcriptional wiring of energy metabolism and combats nitrosative stress. Biochem J 473:693-701.

60. Wagstaff JL, Taylor SL, Howard MJ. 2013. Recent developments and applications of saturation transfer difference nuclear magnetic resonance (STD NMR) spectroscopy. Mol Biosyst 9:571-7.

61. Anonymous. 2015. Mutlibase for Microsoft Excel, Numerical Dynamics, Japan, NumericalDynamics.Com.

Supplementary data:

Supplementary Figure 1: Compound code key

KEGG ID to Compound name conversion table for use with figures 6 and 10.

Supplementary Figure 2: Staining of *Cryptosporidium* in faecal samples

Aniline-carbol-methyl violet stain of a faecal smear taken from a mouse in the infection group. The abundant presence of *Cryptosporidium* (arrows) indicates that the infection has been successful; and that the animal is producing oocysts. These samples were acquired at seven days post-infection.

Supplementary Video 1: Animation of cellular staining of *Cryptosporidium* using confocal microscopy

3D-stacked animation displaying the localisation of Crypt-a-glo (green), MitoTracker (red) and DAPI (blue) in a 3D rendering of 31 individual, 0.16 µm thick sections, overlapping with a final representative thickness of 4.8 µm, displayed in **Figure 1b.**

Supplementary Video 2: Animation of cellular staining of *Cryptosporidium* using confocal microscopy

3D-stacked animation displaying the localisation of Crypt-a-glo (green), MitoTracker (red) and DAPI (blue) in a 3D rendering of 31 individual, 0.16 µm thick sections, overlapping with a final representative thickness of 4.8 µm, displayed in **Figure 1c.**

Supplementary Video 3: Animation of cellular staining of *Cryptosporidium* using confocal microscopy

3D-stacked animation displaying the localisation of Crypt-a-glo (green), MitoTracker (red) and DAPI (blue) in a 3D rendering of 31 individual, 0.16 µm thick sections, overlapping with a final representative thickness of 4.8 µm, displayed in **Figure 1d.**

724 **Figures:**

725 **Figure 1**

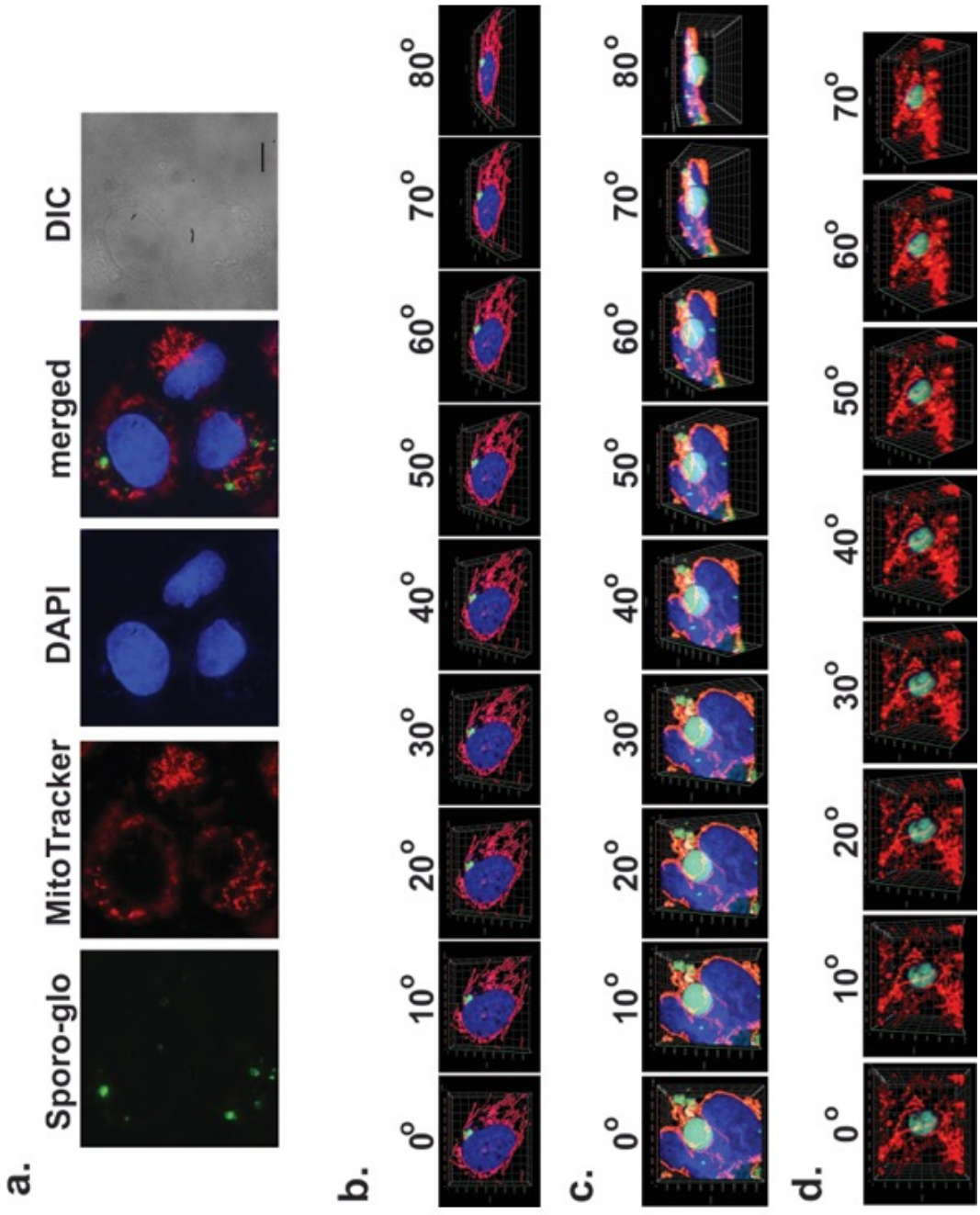

726

Figure 1: Indirect Fluorescence Assay of infected cell cultures

a. Fluorescence microscopy showing the staining of infected COLO-680N culture with Sporo-glo (green), MitoTracker CMXRos (red) and DAPI nuclear stain (blue). From the figure we could observe an obvious mitochondrial "clumping" and polarisation towards areas of infection, suggesting that the presence of the parasite within a host cell affects the positioning of host mitochondria or that host mitochondrial concentration somehow plays a role in determining the site of parasitism. Scale bar: 20 μm **b**. Confocal microscopy showing the localisation of Crypt-a-glo (green), MitoTracker (red) and DAPI (blue) in a 3D rendering of 31 individual, 0.16 μm thick sections, overlapping with a final representative thickness of 4.8 μm. The images are rotated around the x-axis, from 0^{o} to 80^{o}, showing a COLO-680N cell infected with *C. parvum* (green). Individual images of the stainings were captured in different angles, to show the infection on a three-dimensional level. A whole video showing a 360^{o} rotation of the three-dimensional z-stack of the image is found as an animation in **Supplementary Video 1**. **c**. Confocal microscopy showing the localisation of Crypt-a-glo (green), MitoTracker (red) and DAPI (blue) in a 3D rendering of 55 individual, 0.16 μm thick sections, overlapping with a final representative thickness of 8.6 μm. The images are rotated around the x-axis, from 0^{o} to 80^{o}, showing a COLO-680N cell infected with *C. parvum* (green). Individual images of the stainings were captured in different angles, to show the infection on a three-dimensional level. A whole video showing a 360^{o} rotation of the three-dimensional z-stack of the image is found as an animation in **Supplementary Video 2**. **d**. Confocal microscopy showing the localisation of Crypt-a-glo (green) and MitoTracker (red) in a 3D rendering of 51 individual, 0.16 μm thick sections, overlapping with a final

representative thickness of 8.0 µm. The images are rotated around the x-axis, from 0^{o} to 70^{o}, showing mitochondria surrounding an intracellular stage of with *C. parvum* (green). Individual images of the stainings were captured in different angles, to show the infection on a three-dimensional level. A whole video showing a 360^{o} rotation of the three-dimensional z-stack of the image is found as an animation in **Supplementary Video 3**.

Figure 2

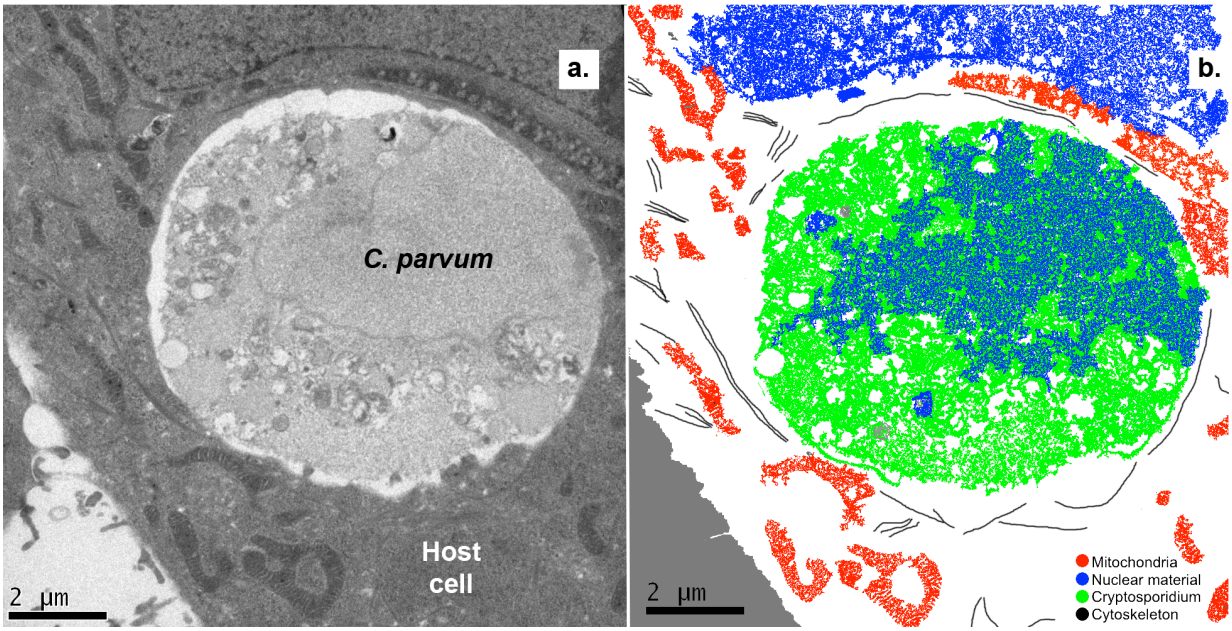

Figure 2: Electron microscopy of *Cryptosporidium* infected host cells.

a. Infection of a host cell by *C. parvum*. Mitochondria of the host cell appear to closely associate with the parasitophorous vacuole surrounding the parasite, while cytoskeletal structures appear to be associated with the organelles. **b.** Cartoon of image a. demonstrating the presence of mitochondria, cytoskeleton, nuclear material and *Cryptosporidium.*

Figure 3

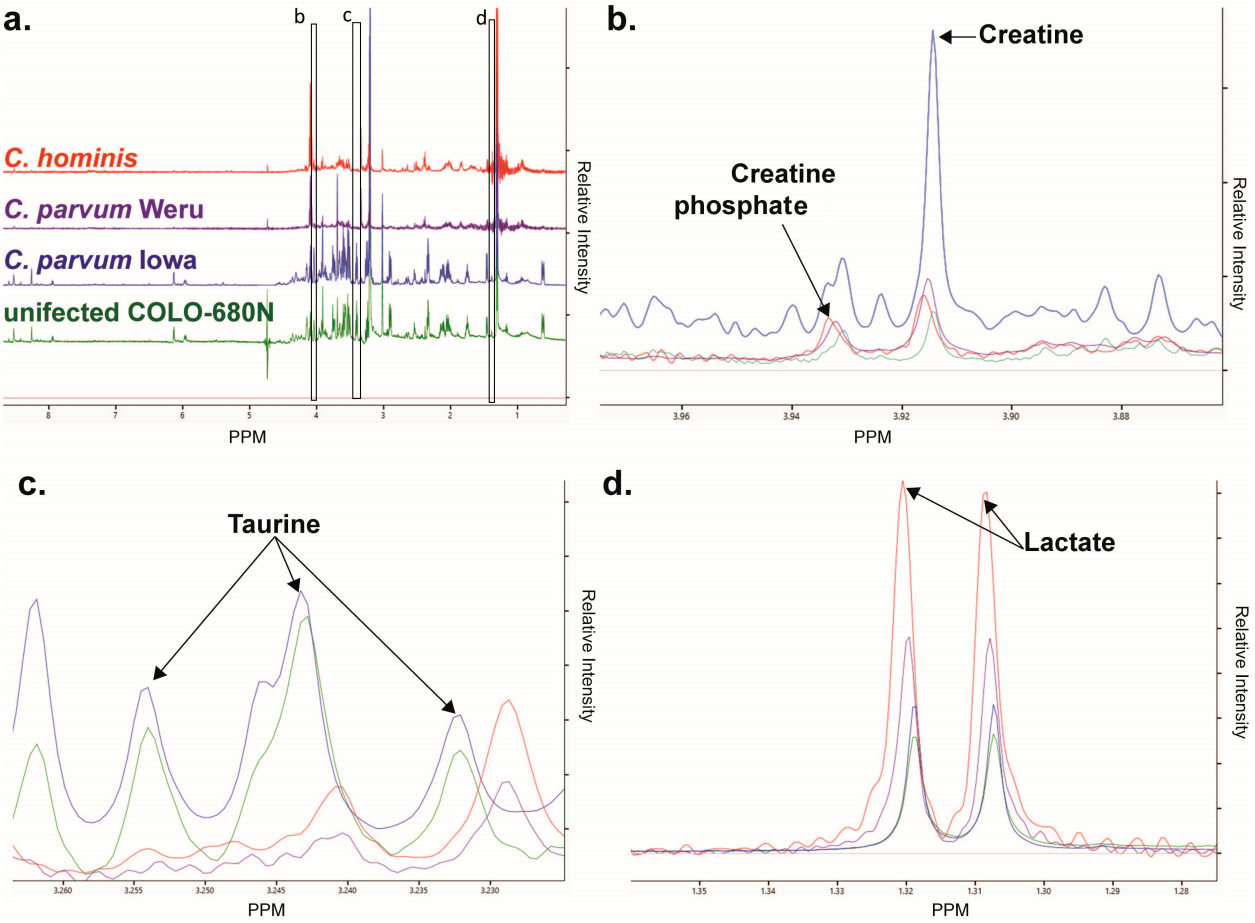

Figure 3: Cell Culture infection NMR spectra

a. Stacked NMR Spectra produced from the COLO-680N control cultures (green), either the *C. parvum* Iowa II (blue), *C. parvum* Weru (purple), or *C. hominis* groups. Direct comparisons of the spectra revealed several clearly identifiably differences, including, again, differences in creatine and creatine phosphate (**b.**), taurine (**c.**) and lactate (**d.**) levels. Noticeably, taurine levels were almost undetectable in *C. hominis* or *C. parvum* Weru infections. The spectra displayed are of individual experiments and are representative of the spectra observed throughout the groups.

Figure 4

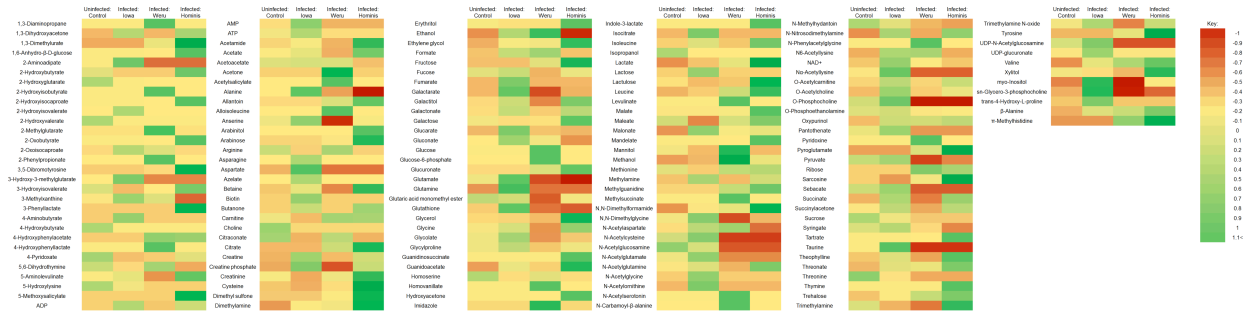

Figure 4: COLO-680N Experiment Metabolites

All the metabolites identified by 1H NMR analysis in infected and uninfected cells were explored via PCA statistical analysis and the resulting Principal Component values of each individual metabolite recorded. The colour coded heat map represents the significance to which each individual metabolite contributed to the identity of the sample groups. Metabolites that contributed towards variation *within* groupings are coded towards the red, whilst green represents metabolites that stayed relative unvaried within groups but demonstrated variation between groups and thus are of most interest. Yellow represents a general lack of variation between or within groups.

Figure 5

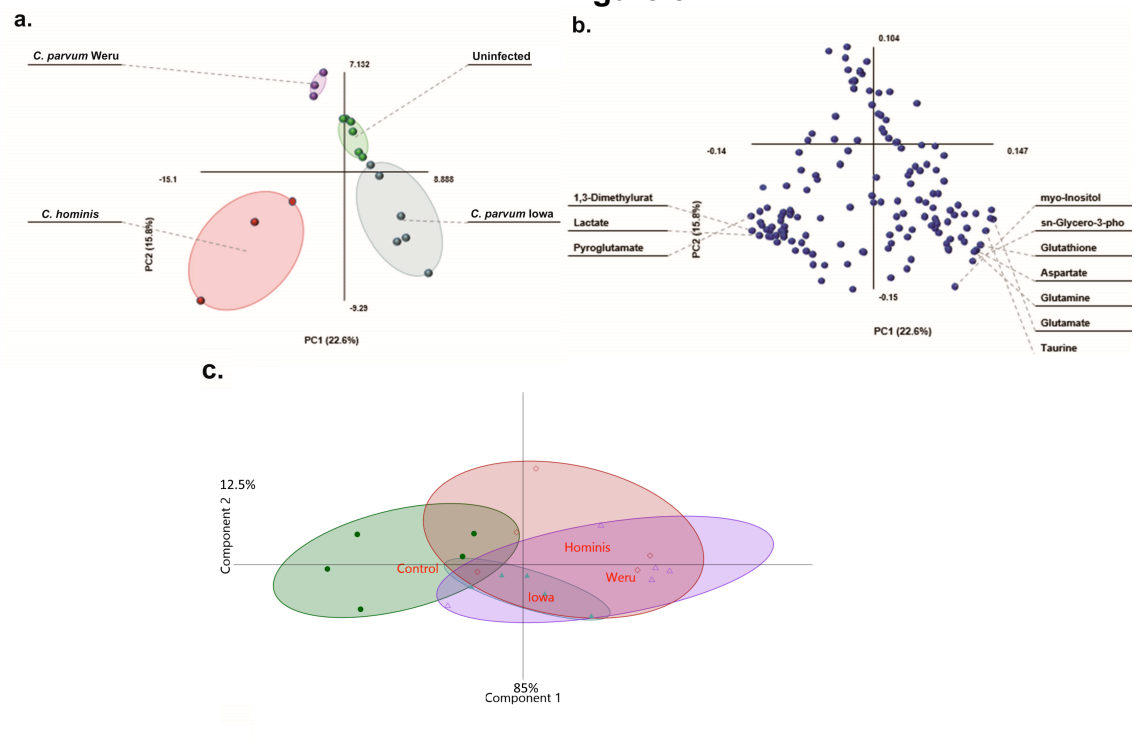

Figure 5: PLS-DA and loading plot of COLO-680N - infected cells NMR results

a. PLS-DA statistical analysis of the information provided by the Chenomx screening produced clear groupings, separating the controls (green), *C. parvum* Iowa II infections (blue), *C. parvum* Weru infections (purple) and *C. hominis* infections (red). As the grouping areas do no overlap the separation between the infection conditions again indicates that metabolome differences can be at least in part explained by different *Cryptosporidium* strains/species. **b.** The loading biplot of the PLS-DA analysis shows lactate as a significant contributor to variation, in addition to taurine and myo-inositol among others. **c.** PLS-DA statistical analysis of the information provided by the Chenomx screening using additional samples, also produced clear groupings, separating the controls (green), *C. parvum* Iowa II infections (blue), *C. parvum* Weru infections (purple) and *C. hominis* infections (red).

Figure 6

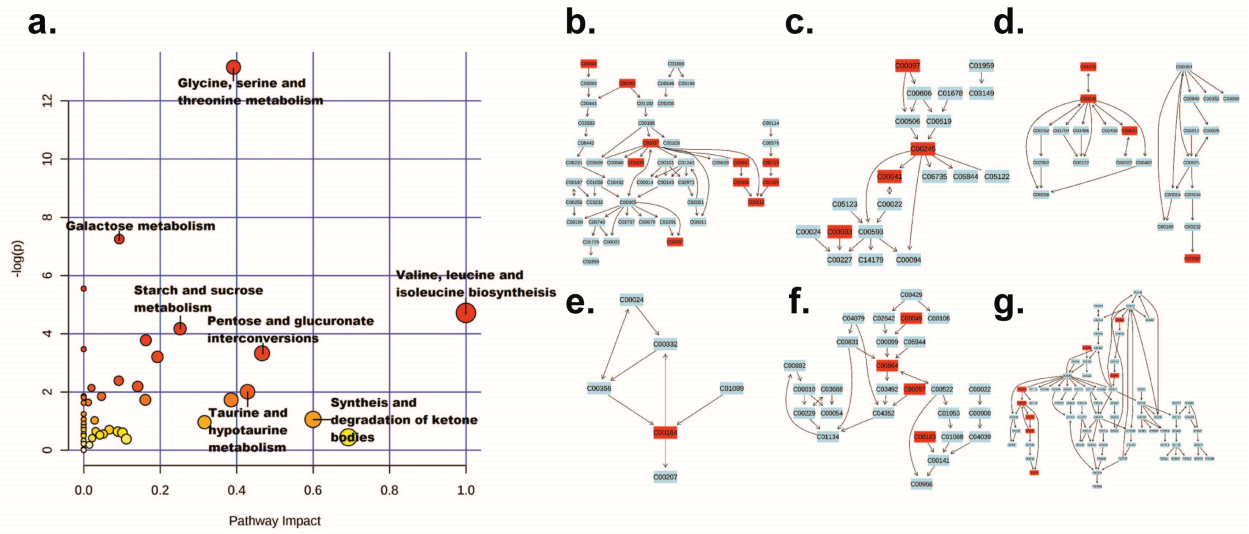

Figure 6: Metabolic pathways detected in cell cultures' NMR samples

a. Data analysed by MetaboAnalyst 3.0, utilising all compounds which displayed some degree of change as a result of infection, produced a graph of pathways most heavily impacted (x axis) and pathways containing the most amount of the given compounds (pathway impact: y-axis), with statistical significance of the predicted pathways increasing as the colour ranges from yellow (low) to red (high). Six pathways were chosen to be of particular interest by their position on the graph, with metabolites present in the experimental samples highlighted in red, including: glycine, serine and threonine metabolism (**b.**), taurine and hypotaurine metabolism (**c.**), Alanine, aspartate and glutamate metabolism (**d.**), synthesis and degradation of ketones (**e.**), pantothenate and CoA biosynthesis (**f.**) and arginine and proline metabolism (**g.**).

Figure 7

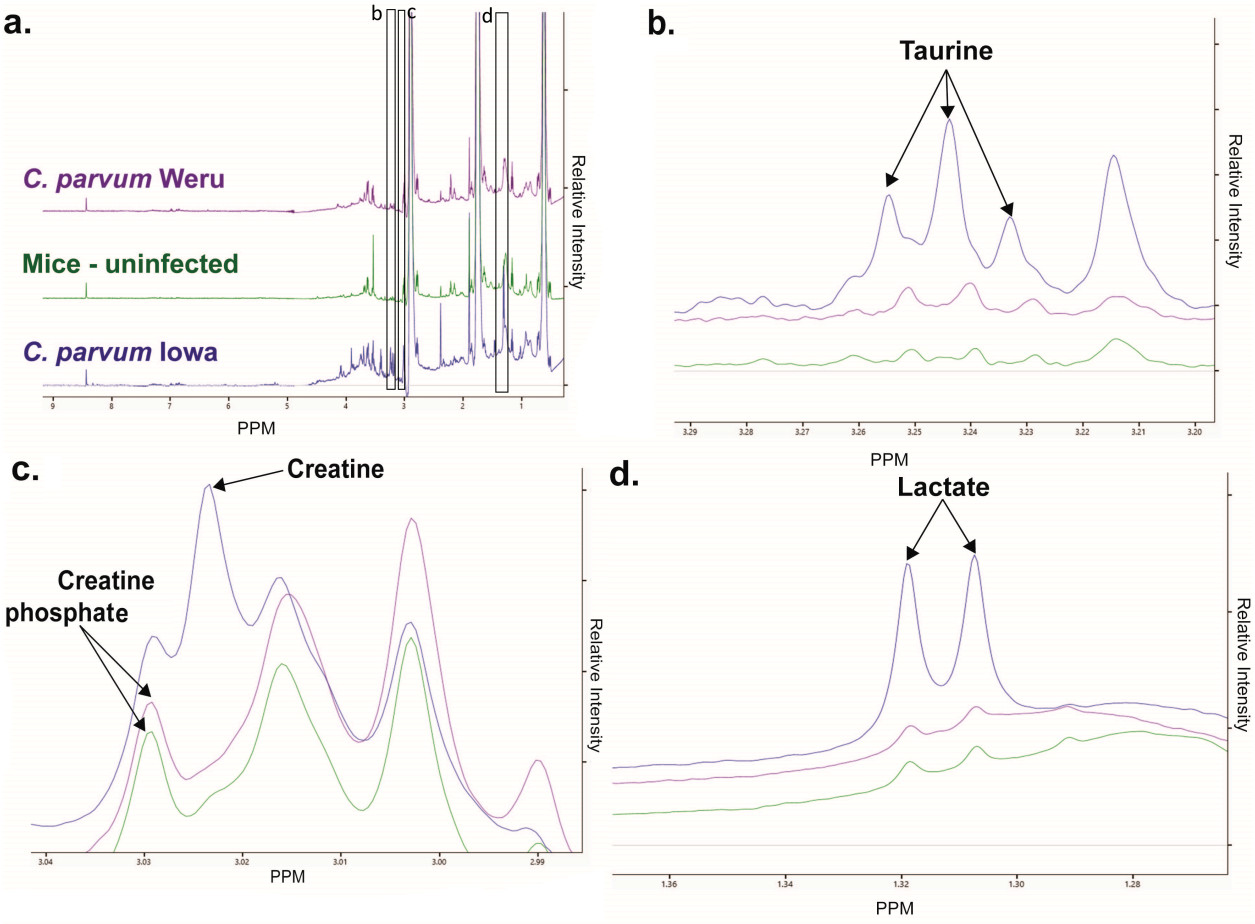

Figure 7: NMR Spectra of mice models of infection

a. Stacked NMR Spectra produced from faecal samples of the control mice (green), or either the Iowa II (blue) or Weru (purple) groups. **b.** Direct comparisons of the spectra revealed several clearly identifiably differences, including differences in creatine and creatine phosphate levels. **c.** Levels of taurine were substantially lower in the control or *C. parvum* Weru samples compared to *C. parvum* Iowa II. **d.** Lactate levels were also much higher in *C. parvum* Iowa II infected mice compared to the barely detectable levels in the control mice or *C. parvum* Weru infected groups.

Figure 8

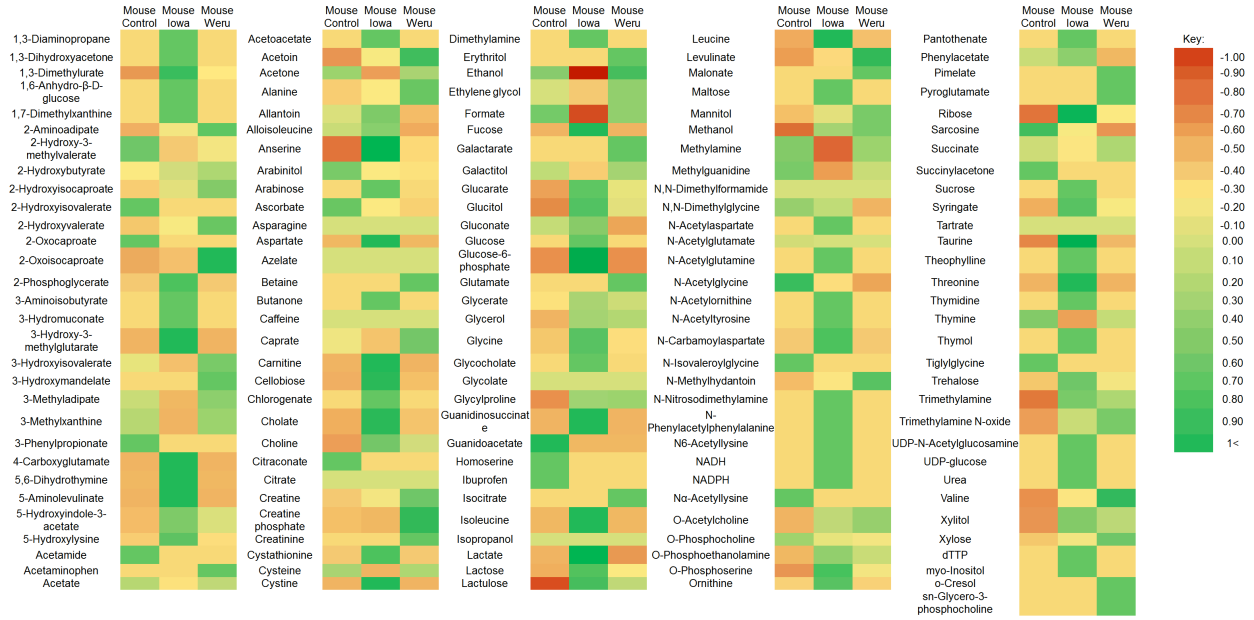

Figure 8: Mice Experiment Metabolites

All the metabolites identified by ^{1}H NMR analysis in infected and uninfected mice were explored via PCA statistical analysis, the Principal Component values for each metabolite were then recorded. Metabolites that contributed towards variation *within* groupings are coded towards the red, whilst green represents metabolites that stayed relative unvaried within groups but demonstrated variation between groups and thus are of most interest. Yellow represents a general lack of variation between or within groups.

Figure 9

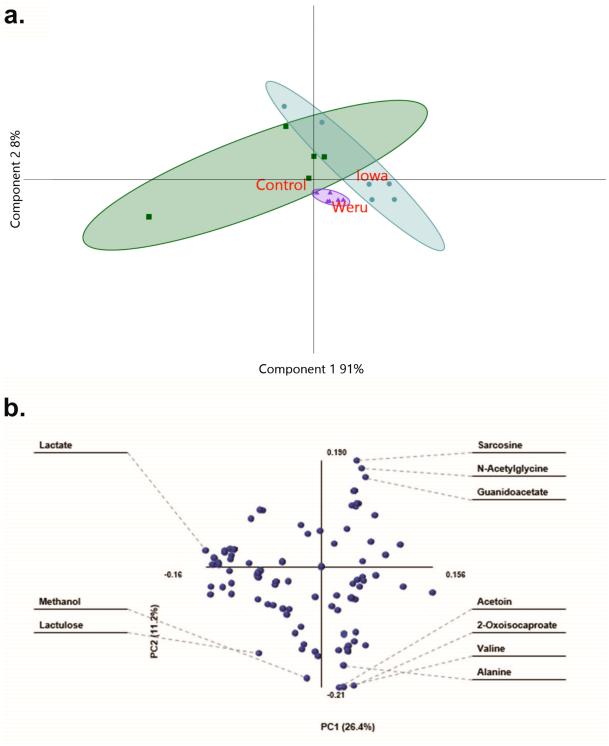

Figure 9: PLS-DA and loading plot of mice model NMR results

a. PLS-DA statistical analysis of the information provided by the Chenomx screening produced clear groupings, separating the controls (green), *C. parvum* Iowa II infections (blue) and *C. parvum* Weru infections (purple). As the grouping areas, indicated by the areas highlighted, do no overlap, it can be said that the separation between the infection conditions represent clear differences in the metabolome, which correspond to the *C. parvum* strain. **b.** The loading biplot of the PLS-DA analysis shows many of the compounds identified by Chenomx contributed towards the separation and groupings. Those on the outer most edges, for example alanine, sarcosine, lactate and lactulose, had some of the greatest influence on the amount of separation as determined by the PLS-DA.

874 **Figure 10**

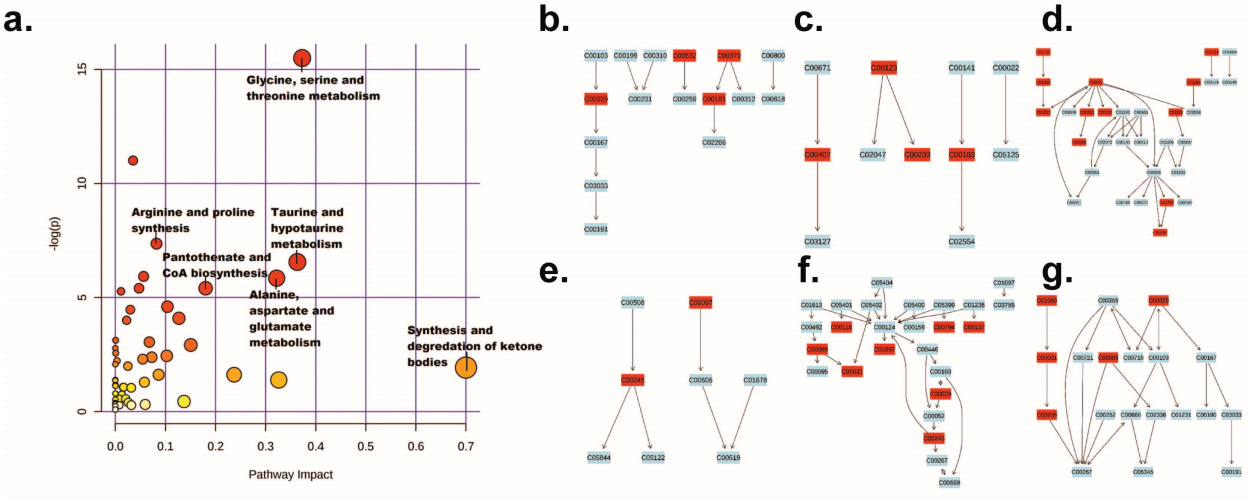

875

876 **Figure 10: Metabolic pathways detected in mouse model NMR samples**

877 **a.** Data analysed by MetaboAnalyst 3.0, utilising all compounds which displayed some
878 degree of change as a result of infection, produced a graph of pathways most heavily
879 impacted (x axis) and pathways containing the most amount of the given compounds
880 (pathway impact: y-axis), with statistical significance of the predicted pathways
881 increasing as the colour ranges from yellow (low) to red (high). Six pathways were
882 chosen to be of particular interest by their position on the graph, with metabolites
883 present in the experimental samples highlighted in red, including: **b.** pentose and
884 glucoronate interconversions, valine, **c.** leucine and isoleucine biosynthesis, **d.** glycine
885 serine and threonine metabolism, **e.** taurine and hypotaurine metabolism, **f.** galactose
886 metabolism and **g.** starch and sucrose metabolism.

887

888

Figure 11

a

Shared changes in C. parvum Iowa II infections				
	Mouse	Cells	Pathways	Function
1,3-Dihydroxyacetone			Glycolysis	Energy supply
3-Hydroxy-3-methylglutarate			Ketogensis	Energy supply
Anserine			Carnosine synthesis	ROS scavenging
Asparagine			Numerous	Numerous
Aspartate			AA Synthesis	
Fucose			N-linked glycosylation	Cell surface signalling
Glycine			Purine synthesis	Numerous
Glycylproline			Collagen synthesis	Connective tissue
Isoleucine			Ketogensisis	Energy supply
N-Acetylaspartate			Numerous	Numerous
N-Acetylornithine			Waste	
N-Nitrosodimethylamine			Carcinogen*	
N6-Acetyllysine			Epigenetics	Gene regulation
Pantothenate			Numerous, CoA synthesis	Numerous, Energy Supply
Syringate			Krebs cycle	Energy supply
Taurine			Numerous	ROS, Osmoregulation
UDP-N-Acetylglucosamine			Sugar synthesis	Cytoskeleton and nuclear pore formation
UDP-glucose			Polysaccharide synthesis	Lipid formation
myo-Inositol			Numerous	Cell signalling andmitochondrial quality control

b

Shared changes in C. parvum Weru infections				
	Mouse	Cells	Pathways	Function
2-Hydroxybutyrate			Cysteine synthesis	Oxidative stress response
Acetone			Ketosis	Energy supply
Citrate			TCA	Energy supply
Creatine			Creatine synthesis	Energy supply
Formate			Folate cycle	Metabolic regulation and methylation
Levulinate			Unknown	Potentially Ketosis based energy supply
Mannitol			Mannitol cycle (Non-mammalian)	Potential parasite energy source
Methylguanidine			Protein catabolism	Regulation of inflammation
Pyroglutamate			Glutathione cycle	Glutatmate storage
Valine			CoA synthesis	Energy Supply

Figure 11: Shared changed in metabolite levels between both cell cultures and mice. Those metabolites which showed a reliable contribution towards group separation in both Mouse and cell culture experiments were recorded and their functions assigned. Those metabolites with established direct or indirect involvement with mitochondria were labelled in red. The analysis was conducted for both the Iowa (a) and Weru (b) infection experiments. *N-Nitrosodimethylamine is a known carcinogen and not naturally produced by any known human or mammalian cell line or any member of the Cryptosporidia and may represent either a contamination or un-characterised spectra peak.